Atomic-resolution chemical imaging of oxygen local bonding environments by electron energy loss spectroscopy

Julia A. Mundy,[1] Qingyun Mao,[1] Charles M. Brooks,[2,3] Darrell G. Schlom,[2,4] and David A. Muller[1,4]
[1]*School of Applied and Engineering Physics, Cornell University, Ithaca, New York 14853, USA*
[2]*Department of Materials Science and Engineering, Cornell University, Ithaca, New York 14853, USA*
[3]*Department of Materials Science and Engineering, Pennsylvania State University, University Park, Pennsylvania 16802, USA*
[4]*Kavli Institute at Cornell for Nanoscale Science, Ithaca, New York 14853, USA*

(Received 19 April 2012; accepted 23 June 2012; published online 26 July 2012)

Electron energy loss spectroscopy on an aberration-corrected scanning transmission electron microscope was used to map the elemental composition and bonding in a thin film of the multiferroic $LuFe_2O_4$ with atomic resolution. A two-dimensional analysis of the fine structure of the O-*K* edge yielded distinct signals for the two inequivalent oxygen sites in the crystal. Comparison to an *ab-initio* simulation showed that these two components can be interpreted in terms of the differing hybridization of the O *p* orbitals to the Lu and Fe *d* orbitals, thus producing an atomic-resolution map of the local oxygen bonding environment. © *2012 American Institute of Physics*. [http://dx.doi.org/10.1063/1.4737208]

Transition metal oxides display a host of properties from ferroelectricity and ferromagnetism to high-temperature superconductivity. While varied in structure and composition, the ubiquitous backbone is the cage of oxygen atoms surrounding the transition metal cation. Small distortions such as tilts and rotations of the oxygen octahedron or tetrahedron can dramatically impact the properties of the material. Current computational studies are attempting to harness these octahedral rotations to engineer materials with desired properties.[1–4] Thus, accurately determining the position and local bonding environment of the oxygen atoms experimentally is crucial in correlating the structure to the macroscopic properties.

Advances in aberration correction[5,6] have made electron energy loss spectroscopy (EELS) on a scanning transmission electron microscope (STEM) a powerful tool for probing elemental concentrations at the atomic scale.[7,8] Current electron microscopes are capable of focusing electron beams to 1 Å to perform scattering experiments as the electrons travel down a single column of atoms in a thin crystalline specimen. For inelastic scattering due to a core-level transition, EELS can provide a chemical fingerprint due to the unique binding energies of each element. In particular, the energy-loss near-edge fine structure (ELNES) from these transitions should track the local density of states (LDOS) above the Fermi level, partitioned by site, chemical species and angular momentum due to the dipole selection rules.[9] For transition metal $L_{2,3}$ edges, however, strong core-hole effects produce a significant deviation between the LDOS and the observed ELNES (Ref. 10); nevertheless, comparison to fingerprint spectra has permitted atomic resolution two-dimensional maps of oxidation state of transition metal and lanthanide cations using EELS.[8,11,12]

In contrast to the transition metal $L_{2,3}$ edges, the oxygen *K* edge ELNES can be more simply related to the LDOS as the oxygen *2p* electrons mostly screen the *1s* core hole.[13] The result is a distorted but often recognizable reflection of the ground state LDOS.[9,13] In a tight-binding decomposition, the bulk of the O *2s* and *2p* states are occupied and thus much of the oscillator strength on the O-*K* edge is composed of states that can be attributed to overlap with the neighboring sites. As such, the O-*K* edge is rich with information about the system and in particular can be sensitive to the number of *d* holes if bonded to transition metals, and more generally the nearest-neighbor bonding to cations, including those for which the EELS edges lie outside the energy range accessible by current spectrometers.[9,14,15] Oxygen spectroscopic images, however, can be difficult to obtain due to the inherently low jump ratio of the edge and often require substantial post-acquisition data processing.[16] This not only can produce artifacts in a concentration map that can be mistaken for channeling contrast, but also alters the fine structure of the EELS signal.[17] Improved optics on the current generation of spectrometers allows for greater collection efficiency and thus more signal, making the O-*K* edge more accessible. Here, we present EELS spectral maps of the oxygen atoms in $LuFe_2O_4$ and probe the local bonding environment through atomic-resolution analysis of the O-*K* edge fine structure. We show that direct maps of the oxygen positions and local environment can be obtained, even in the presence of heavy cations. We find that attempts to enhance the signal using the popular principal components analysis distorted the bonding maps.

We investigate thin films of $LuFe_2O_4$, purported to be the highest temperature known simultaneous ferroelectric ferrimagnet.[18] The ferroelectricity was attributed to charge ordering on the iron sites[18] which allows for a polarization without precluding magnetism. A recent series of studies, however, have suggested that $LuFe_2O_4$ is not ferroelectric[19–21] and that while both Fe^{2+} and Fe^{3+} formal valences are present, the charge arrangements result in a non-polar structure.[20] It is worth noting that while distinct iron valence states have been observed in the bulk[18] and superlattice reflections which could be consistent with

charge ordering have been observed in TEM diffraction,[22] a direct measure of the iron valence atomic column by atomic column remains elusive. $LuFe_2O_4$ has a layered hexagonal structure, $R\bar{3}m$, consisting of planes of Lu-O (U layers[23]) alternating with double planes of Fe-O (W layers[23]). There are two distinct oxygen sites in the crystal.[24] The oxygen atoms that sit slightly above and below the iron planes, "O_1," are surrounded by four iron atoms with a long bond to a lone lutetium atom in an asymmetric trigonal bipyramid structure. In contrast, the remaining oxygen atoms, "O_2," are surrounded by a roughly tetrahedral cage of three lutetium atoms and a single iron atom. The O-*K* edge probes the hybridization of the O *p* orbitals to the Lu and Fe *d* orbitals, thus we can observed distinct EELS fine structure fingerprints from O_1 and O_2. Finally, using atomic resolution EELS we investigate the Fe valence yet fail to identify a consistent charge-ordering pattern in our samples at room temperature, which also do not show the superlattice reflections. We show the valence shift on a single column of Fe atoms can be determined with a precision of $\pm 0.09\,e$ (1 standard deviation), which should be sufficient to test charge ordering patterns in systems where charge ordering has been observed by x-ray diffraction.

Thin films of $LuFe_2O_4$ were grown on (111) $MgAl_2O_4$ by reactive oxide molecular-beam epitaxy in a Veeco GEN 10; x-ray diffraction and magnetic measurements are reported elsewhere.[25] Spectroscopic images of cross-sectional TEM specimens were performed on a 100 keV Nion UltraSTEM, a 5th order aberration corrected microscope optimized for EELS spectroscopic imaging with a probe size of 1 Å, EELS energy resolution of 0.6 eV and a high usable beam current. Simultaneous maps of Lu, Fe, and O were acquired with a 1 eV/channel dispersion and maps revealing fine structure with 0.3 eV/channel. Calculations of the EELS fine structure of $LuFe_2O_4$ (Ref. 24) were performed with FEFF9 (Refs. 26 and 27) with 100 keV incident electrons, convergence and collection angles of 30 and 80 mrad, respectively, to match the experimental conditions. Core-hole effects, and a 0.2 eV energy broadening were included. Ground state LDOS were also calculated using

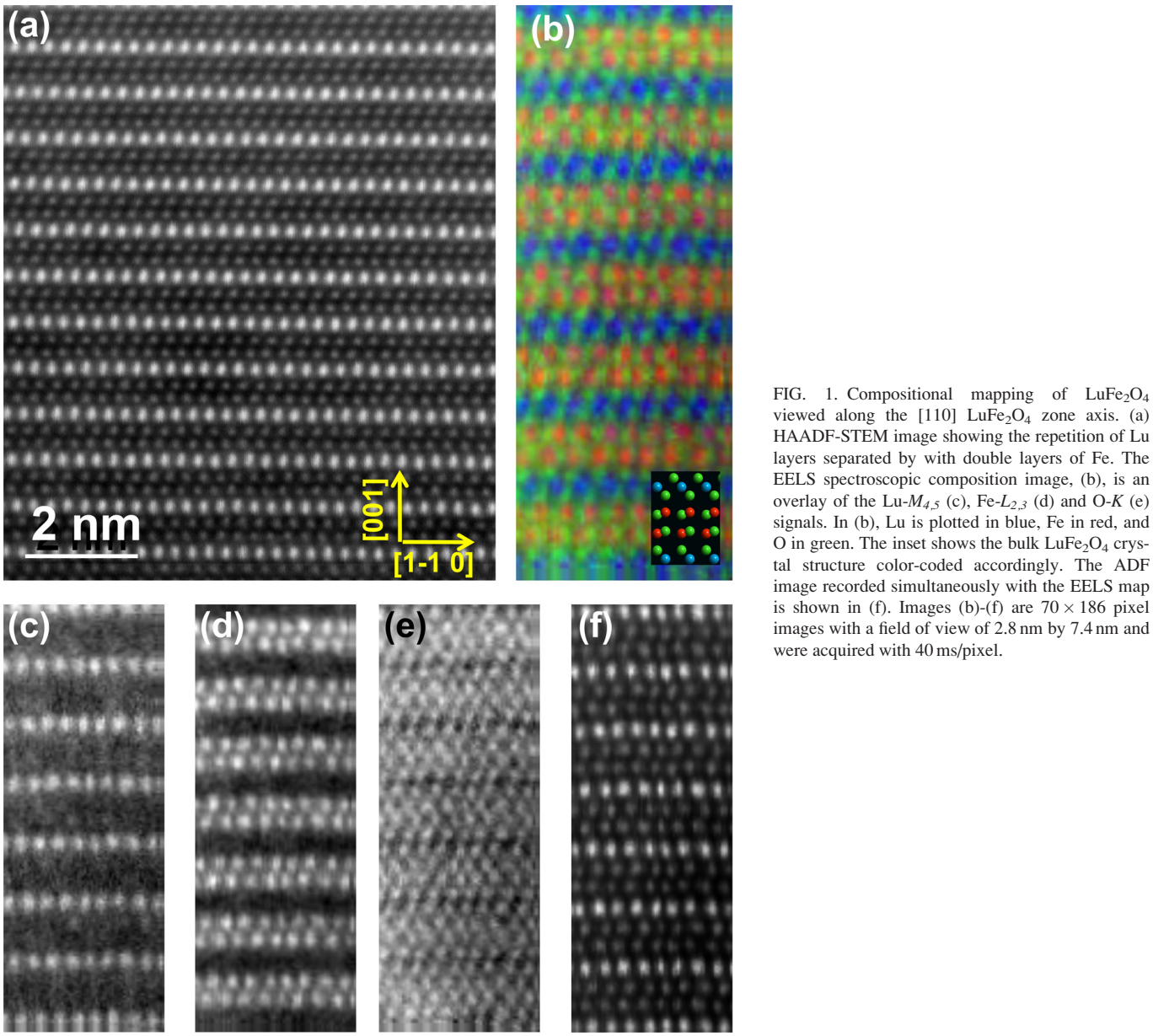

FIG. 1. Compositional mapping of $LuFe_2O_4$ viewed along the [110] $LuFe_2O_4$ zone axis. (a) HAADF-STEM image showing the repetition of Lu layers separated by with double layers of Fe. The EELS spectroscopic composition image, (b), is an overlay of the Lu-$M_{4,5}$ (c), Fe-$L_{2,3}$ (d) and O-*K* (e) signals. In (b), Lu is plotted in blue, Fe in red, and O in green. The inset shows the bulk $LuFe_2O_4$ crystal structure color-coded accordingly. The ADF image recorded simultaneously with the EELS map is shown in (f). Images (b)-(f) are 70×186 pixel images with a field of view of 2.8 nm by 7.4 nm and were acquired with 40 ms/pixel.

Wien 2k, which provides a more accurate treatment of the near-edge features.[28,29]

Figure 1 shows a two-dimensional atomic resolution spectroscopic image of $LuFe_2O_4$ oriented along the [110] zone axis of the film. The film is single phase and well ordered as shown in the high angle annular dark field (HAADF-STEM) image, Fig. 1(a). The EELS spectroscopic image, Figs. 1(b)–1(e), simultaneously resolves the atomic positions of all the elements in the film using the Lu-$M_{4,5}$, Fe-$L_{2,3}$, and O-K edges. The simultaneously recorded ADF signal is shown for comparison in Fig. 1(f). The concentrations plotted are obtained using a simple power law background subtraction and integration over the edge without additional noise reduction techniques. A small amount of intermixing between the iron and lutetium sublattices is observed in the EELS map. This may reflect step edges viewed in projection or genuine anti-site defects. Finally, as test of sensitivity, we note that the oxygen atoms sit 0.25 Å above and below the iron atoms in the Fe-O planes in the bulk crystal structure[24]—this is clearly apparent in overlaid image, Fig. 1(b).

In addition to mapping the concentration of oxygen atoms, the fine structure of the O-K edge can be used to map the local bonding environment with atomic resolution as shown in Fig. 2. The oxygen signal, integrated in Fig. 2(b), was extracted from a representative region of the film, shown in Fig. 2(a). Analysis of the fine structure of the EELS signal produced two distinct components, shown in Fig. 2(c). A non-negative non-linear least squares fit of these components to the full spectrum map, Fig. 2(d), reveals the oxygen fine structure is clearly bifurcated into distinct concentrations of oxygen atoms in the Fe-O layers, O_1, and those in the Lu-O layers, O_2. Finally, we note that all analysis was performed without the application of the popular weighted principal component analysis (w-PCA) filter.[30] We find the use of the filter severely distorts the concentration maps (Supplementary Fig. S1 of Ref. 31) even when an excess of components well beyond that suggested by the screen-plot criterion are used. Similar artifacts have been observed for one-dimensional concentration profiles.[17] These artifact are reminiscent of those observed in previous attempts to map the local bonding structure with oxygen which was attributed to fundamental limitations from channeling, delocalization and thermal diffuse scattering.[32] Here we show that at moderate sample thicknesses these need not be fundamental limits and direct maps can be obtained, even in the presence of heavy elements. We would caution against using PCA filtering on raw data, especially when the peak-background ratio (or signal/noise ratio as defined in Ref. 7) is low.

To understand the origin of the peaks, simulations with FEFF9 were performed. FEFF is an *ab-initio* self-consistent multiple-scattering code based on a real space Green's function approach that calculates the excitation spectra and electronic structure in the presence of a core hole.[26,27] Because we do not detect the characteristic (1/3,1/3,half integer) diffraction peaks characteristic of structural charge ordering in our samples, we model the system in the unordered state where the all the iron sites have the same oxidation state.[33] Unlike previous cluster calculations for this system, the iron oxidation state is consistent for all sites.[34] FEFF computes the extended fine structure over a wide energy range, though is less accurate for the very near edge structure, especially for the first few eV of the edge due to its sensitivity to the position of the Fermi energy as a result of errors inherent in its use of the muffin tin potentials. For this reason, we checked our results with full-potential calculations using Wien 2k and again saw similar trends[28] as shown in Supplementary Fig. S2 of Ref. 31. We did not include a core hole in the Wien 2k calculations, indicating that the trends shown in Fig. 3 persist in the ground state.

The O p, Lu d, and Fe d density of states for the distinct oxygen sites O_1 and O_2 are shown in Figs. 3(a) and 3(b),

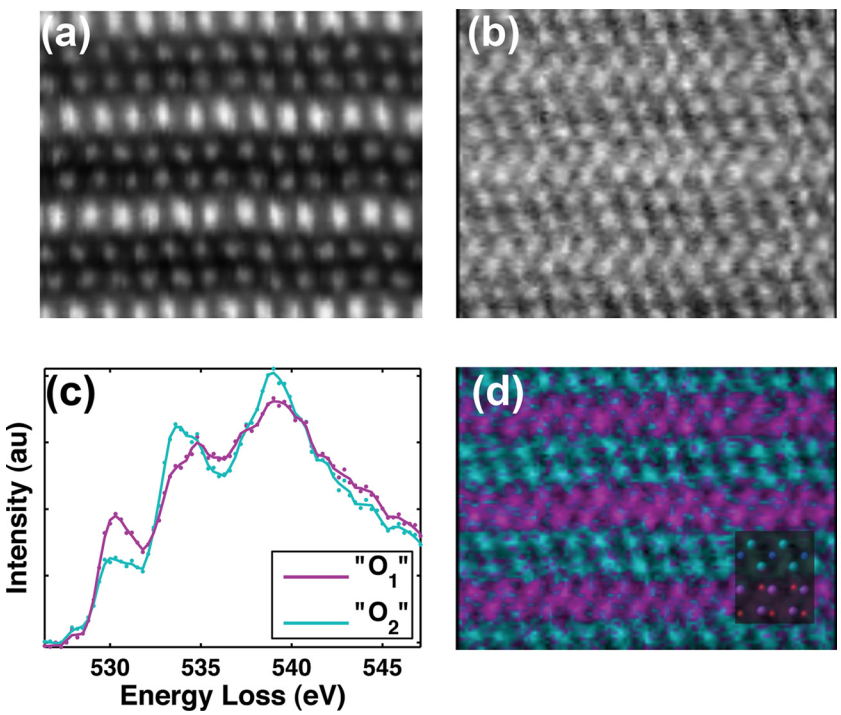

FIG. 2. Local bonding information extracted from the O-K edge. (a) HAADF-STEM image recorded simultaneously with the O concentration map of (b). Two distinct components were present in the O-K edge fine structure, (c), and fit to the spectroscopic image as shown in (d). The inset to (d) shows the crystal structure Fe plotted in red, Lu in blue, and "O_1" and "O_2" in magenta and turquoise respectively. (a), (b), and (d) are 123×91 pixel images with a field of view of 3.4 nm by 2.5 nm and were acquired with 40 ms/pixel.

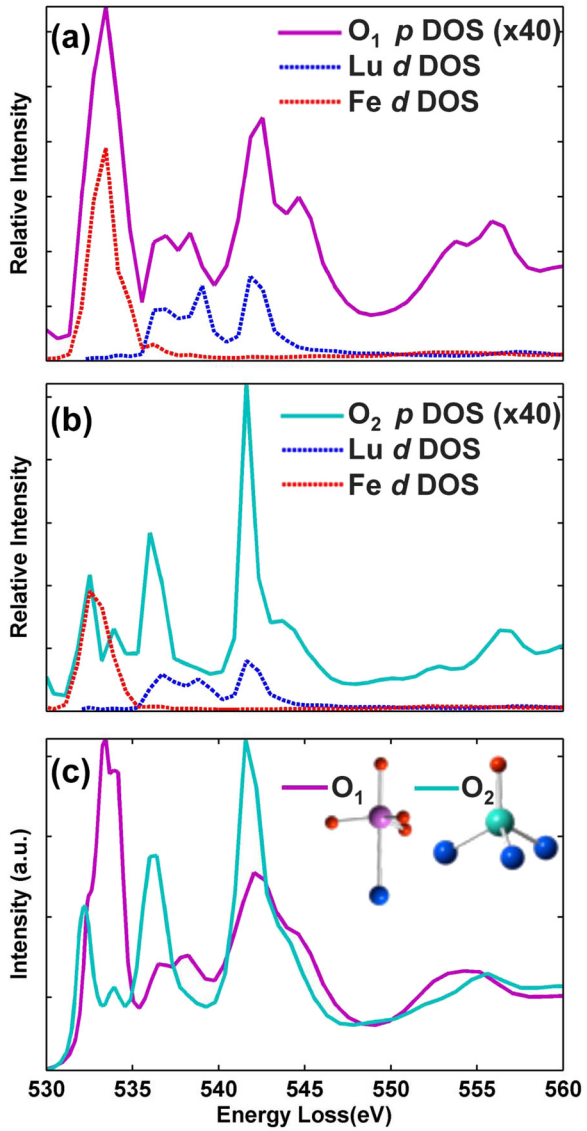

FIG. 3. FEFF calculations of the EELS fine structure. The O *p* and Lu and Fe *d* local densities of states are shown for the distinct O_1 and O_2 sites in (a) and (b), respectively. In both cases, the much weaker O *p* LDOS tracks the combined Fe and Lu LDOS. The corresponding calculated EELS signal is shown in (c). A cartoon inset to (c) shows the local chemical environment of O_1 and O_2. Lu is plotted in blue, Fe in red, and the O atom in magenta and turquoise, respectively.

respectively. The resulting EELS spectra are shown in Fig. 3(c). The first peak at ~533 eV, corresponding to the hybridization of the O *p* orbitals to the Fe *d* orbitals, is distinct for the two oxygen sites. As shown in the inset to Fig. 3(c), O_1 has four iron nearest neighbors in contrast to one for O_2. The calculated EELS signal in Fig. 3(c), as well as the experimentally recorded spectra in Fig. 2(c), shows a much stronger feature for the O_1 spectra in this energy range. In contrast, the second two peaks are primarily due to the overlap of the Lu *d* orbitals with the O *p* orbitals. Here, O_2 has three Lu nearest neighbors whereas O_1 has one, resulting in a stronger peak in this region for the O_2 spectra. Thus the signal can be used as a local fingerprint for the orbital hybridization between the O atom and the surrounding cations. We have seen similar trends in non-spatially resolved measurements for the substitution of *A*-site cations in bulk perovskites,[14] but here the measurements and observed changes are local and site specific.

Finally, given that EELS is capable of probing bonding information with atomic resolution, we turn to investigate the sensitivity of EELS to proposed charge ordering arrangements on the iron sites. Similar to other transition metal cations, the Fe $L_{2,3}$-edge is sensitive to the valence with the onset energy shifting as the oxidation changes from +2 to +3.[10,12] We image $LuFe_2O_4$ down the [1 $\bar{1}$ 0] zone axis of the crystal;[22] to increase the signal-to-noise, a full spectrum map was acquired, the Fe sites identified from the simultaneous ADF image and a mean spectrum generated from each atomic column. When these spectra are fit with "Fe^{+2}" and "Fe^{+3}" references, only small fluctuations (a standard deviation of 0.09 *e*) around a mean valence are observed as is shown in Fig. 4. Notably, no consistent, reproducible charge-ordering pattern was discerned for our room temperature measurements in these films. This is consistent with the absence of ferroelectricity observed in the thin film by second harmonic generation measurements.[35] This also justifies the use of a single mean iron oxidation state for our calculations.

In summary, we have obtained atomic-resolution EELS spectroscopic images of all atomic species in a thin film of the multiferroic $LuFe_2O_4$. The EELS O-*K* edge fine structure was used to map changes in electronic structure in two-dimensions with atomic resolution, describing the local

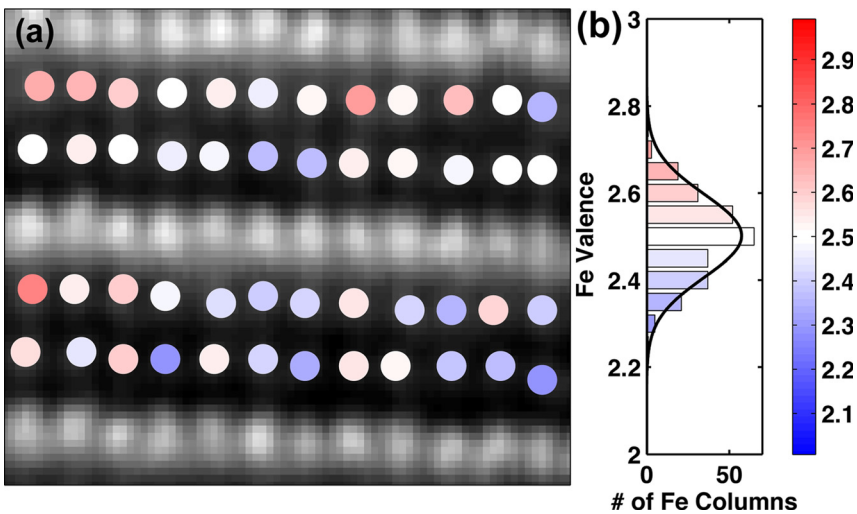

FIG. 4. Measurement of the Fe oxidation state down [1 $\bar{1}$ 0] zone axis of the film. (a) ADF image on which the Fe valence obtained from an analysis of the Fe-$L_{2,3}$ edge fine structure is overlaid. Blue is used to indicate pure Fe^{+2} and red, pure Fe^{+3}. No consistent charge ordering pattern is observed. (b) A histogram of Fe valences from all rows of panel (a) as well as other spectroscopic images with the same acquisition parameters (272 total Fe columns), showing a unimodal Gaussian distribution with a standard deviation of 0.09 *e*, placing a bound on the detection sensitivity for charge modulations, which should produce a bimodal distribution.

coupling of the oxygen 2*p* orbitals to the Fe and Lu *d* orbitals. Atomic-resolution mapping of the fine structure in the O-*K* edge should lend insight for other transition metal oxides. In particular, while Lu and Fe both had an accessible EELS edge, the O-*K* edge can also track nearest neighbor bonding to cations that have inaccessible EELS edges either due to overlap with another edge or a weak cross section as is the case for Sr, Ru, W, and Bi. Thus, the O-*K* edge fine structure analysis could provide an alternative pathway to mapping the concentrations of these elements in materials such as $BiFeO_3$ or $SrRuO_3$. Finally, while atomic-resolution valence mapping with a sensitivity of 0.09 *e* on the Fe sites did not show a consistent charge-ordering pattern in our sample, the demonstrated spatial resolution and valence sensitivity should prove useful for future exploring the O *K*-edge or the Fe charge ordering with EELS at low temperatures where the valence modulations should be more pronounced.

Research supported by the U.S. Department of Energy, Office of Basic Energy Sciences, Division of Materials Sciences and Engineering under Award #DE-SC0002334. This work made use of the electron microscopy facility of the Cornell Center for Materials Research (CCMR) with support from the National Science Foundation Materials Research Science and Engineering Centers (MRSEC) program (DMR 1120296) and NSF IMR-0417392. JAM acknowledges financial support from the Army Research Office in the form of a National Defense Science & Engineering Graduate Fellowship. CMB acknowledges stipend support from the National Science Foundation through the MRSEC program (DMR-0820404).

[1]N. A. Benedek and C. J. Fennie, Phys. Rev. Lett. **106**, 107204 (2011).
[2]J. M. Rondinelli and C. J. Fennie, Adv. Mater. **24**, 1918–1918 (2012).
[3]J. M. Rondinelli, S. J. May, and J. W. Freeland, MRS Bull. **37**, 261–270 (2012).
[4]A. T. Mulder, N. A. Benedek, J. M. Rondinelli, and C. J. Fennie, Arxiv preprint arXiv:1205.5526 (2012).
[5]P. E. Batson, N. Dellby, and O. L. Krivanek, Nature **418**, 617–620 (2002).
[6]H. Muller, S. Uhlemann, P. Hartel, and M. Haider, Microsc. Microanal. **12**, 442–455 (2006).
[7]G. A. Botton, S. Lazar, and C. Dwyer, Ultramicroscopy **110**, 926–934 (2010).
[8]D. A. Muller, L. F. Kourkoutis, M. Murfitt, J. H. Song, H. Y. Hwang, J. Silcox, N. Dellby, and O. L. Krivanek, Science **319**, 1073–1076 (2008).
[9]P. Rez and D. A. Muller, Annu. Rev. Mater. Res. **38**, 535–558 (2008).
[10]R. Leapman and L. Grunes, Phys. Rev. Lett. **45**, 397–401 (1980).
[11]J. H. Lee, L. Fang, E. Vlahos, X. Ke, Y. W. Jung, L. F. Kourkoutis, J.-W. Kim, P. J. Ryan, T. Heeg, M. Roeckerath, V. Goian, M. Bernhagen, R. Uecker, P. C. Hammel, K. M. Rabe, S. Kamba, J. Schubert, J. W. Freeland, D. A. Muller, C. J. Fennie, P. Schiffer, V. Gopalan, E. Johnston-Halperin, and D. G. Schlom, Nature **466**, 954–958 (2010).
[12]H. Tan, S. Turner, E. Yücelen, J. Verbeeck, and G. Van Tendeloo, Phys. Rev. Lett. **107**, 107602 (2011).
[13]J. Van Elp and A. Tanaka, Phys. Rev. B **60**, 5331 (1999).
[14]L. F. Kourkoutis, H. Xin, T. Higuchi, Y. Hotta, J. Lee, Y. Hikita, D. Schlom, H. Hwang, and D. A. Muller, Philos. Mag. **90**, 4731–4749 (2010).
[15]H. Kurata, E. Lefevre, C. Colliex, and R. Brydson, Phys. Rev. B **47**, 13763 (1993).
[16]M. Varela, M. P. Oxley, W. Luo, J. Tao, M. Watanabe, A. R. Lupini, S. T. Pantelides, and S. J. Pennycook, Phys. Rev. B **79**, 085117 (2009).
[17]P. Cueva, R. Hovden, J. A. Mundy, H. L. Xin, and D. A. Muller, Microsc. Microanal. **FirstView**, 1–9 (2012).
[18]N. Ikeda, H. Ohsumi, K. Ohwada, K. Ishii, T. Inami, K. Kakurai, Y. Murakami, K. Yoshii, S. Mori, Y. Horibe, and H. Kito, Nature **436**, 1136–1138 (2005).
[19]A. Ruff, S. Krohns, F. Schrettle, V. Tsurkan, P. Lunkenheimer, and A. Loidl, Arxiv preprint arXiv:1204.1244 (2012).
[20]J. de Groot, T. Mueller, R. A. Rosenberg, D. J. Keavney, Z. Islam, J. W. Kim, and M. Angst, Phys. Rev. Lett. **108**, 187601 (2012).
[21]J. de Groot, K. Marty, M. D. Lumsden, A. D. Christianson, S. E. Nagler, S. Adiga, W. J. H. Borghols, K. Schmalzl, Z. Yamani, S. R. Bland, R. de Souza, U. Staub, W. Schweika, Y. Su, and M. Angst, Phys. Rev. Lett. **108**, 037206 (2012).
[22]Y. Zhang, H. X. Yang, C. Ma, H. F. Tian, and J. Q. Li, Phys. Rev. Lett. **98**, 247602 (2007).
[23]T. Sugihara, K. Siratori, N. Kimizuka, J. Iida, H. Hiroyoshi, and Y. Nakagawa, J. Phys. Soc. Jpn. **54**, 1139–1145 (1985).
[24]M. Isobe, N. Kimizuka, J. Iida, and S. Takekawa, Acta Crystallogr. **C46**, 1917–1918 (1990).
[25]C. M. Brooks, R. Misra, J. A. Mundy, L. A. Zhang, B. S. Holinsworth, K. R. O'Neal, T., W. Z. Heeg, J. Schubert, J. L. Musfeldt, Z.-K. Liu, D. A. Muller, P. Schiffer, and D. G. Schlom, "The adsorption-controlled growth of $LuFe_2O_4$ by molecular-beam epitaxy" (unpublished).
[26]J. J. Rehr and R. C. Albers, Rev. Mod. Phys. **72**, 621–654 (2000).
[27]J. J. Rehr, J. J. Kas, M. P. Prange, A. P. Sorini, Y. Takimoto, and F. Vila, C. R. Phys. **10**, 548–559 (2009).
[28]P. Blaha, K. Schwarz, G. Madsen, D. Kvasicka, and J. Luitz, *WIEN2k: An augmented plane wave + local orbitals program for calculating crystal properties* (Technical University of Vienna, Vienna, 2001).
[29]C. Hebert, Micron **38**, 12–28 (2007).
[30]M. Bosman, M. Watanabe, D. Alexander, and V. Keast, Ultramicroscopy **106**, 1024–1032 (2006).
[31]See supplementary material at http://dx.doi.org/10.1063/1.4737208 for the weighted PCA analysis and Wein2k calculations.
[32]M. Haruta, K. Kurashima, T. Nagai, H. Komatsu, Y. Shimakawa, H. Kurata, and K. Kimoto, Appl. Phys. Lett. **100**, 163107 (2012).
[33]H. Xiang and M. H. Whangbo, Phys. Rev. Lett. **98**, 246403 (2007).
[34]K. T. Ko, H. J. Noh, J. Y. Kim, B. G. Park, J. H. Park, A. Tanaka, S. B. Kim, C. L. Zhang, and S. W. Cheong, Phys. Rev. Lett. **103**, 207202 (2009).
[35]E. Barnes and V. Gopalan, private communication (2012).